This article has been accepted for publication in IEEE/OSA Journal of Lightwave Technology. This is the author's version which has not been fully edited and content may change prior to final publication. Citation information: DOI 10.1109/JLT.2023.3319166



# Field Trial of Coexistence and Simultaneous Switching of Real-Time Fiber Sensing and Coherent 400 GbE in a Dense Urban Environment

Zehao Wang, Yue-Kai Huang, Ezra Ip, Zhenzhou Qi, Gil Zussman, Dan Kilper, Koji Asahi, Hideo Kageshima, Yoshiaki Aono, and Tingjun Chen

*(Top-Scored Paper)*

***Abstract*—Recent advances in optical fiber sensing have enabled telecom network operators to monitor their fiber infrastructure while generating new revenue in various application scenarios including data center interconnect, public safety, smart cities, and seismic monitoring. However, given the high utilization of fiber networks for data transmission, it is undesirable to allocate dedicated fiber strands solely for sensing purposes. Therefore, it is crucial to ensure the reliable coexistence of fiber sensing and communication signals that co-propagate on the same fiber. In this paper, we conduct field trials in a reconfigurable optical add-drop multiplexer (ROADM) network enabled by the PAWR COSMOS testbed, utilizing metro area fibers in Manhattan, New York City. We verify the coexistence of real-time constant-amplitude distributed acoustic sensing (DAS), coherent 400 GbE, and analog radio-over-fiber (ARoF) signals. Measurement results obtained from the field trial demonstrate that the quality of transmission (QoT) of the coherent 400 GbE signal remains unaffected during co-propagation with DAS and ARoF signals in adjacent dense wavelength-division multiplexing (DWDM) channels. In addition, we present a use case of this coexistence system supporting preemptive DAS-informed optical path switching before link failure.**

***Index Terms*—Integrated fiber sensing and communication, coexistence, distributed acoustic sensing, coherent transmission, optical switching, field trial.**

Manuscript received June 1, 2023; revised August 4, 2023; accpeted September 8, 2023. A preliminary version of this paper was presented at the IEEE/Optica Optical Fiber Communication Conference (OFC'23), Mar. 2023 [1]. This work was supported by NSF grants CNS-1827923, EEC-2133516, OAC-2029295, CNS-2128638, CNS-2211944, CNS-2330333, and Science Foundation Ireland under Grant #13/RC/2077_P2. This work was also supported in part by NSF grant CNS-2148128 and by funds from federal agency and industry partners as specified in the Resilient & Intelligent NextG Systems (RINGS) program. Z. Wang and Y.-K. Huang contributed equally to this work and should be considered co-first authors.

Z. Wang is with NEC Laboratories America, Princeton, NJ 08540, USA, and the Department of Electrical and Computer Engineering, Duke University, Durham, NC 27708, USA (email: zehao.w@duke.edu).

Y.-K. Huang and E. Ip are with NEC Laboratories America, Princeton, NJ 08540, USA (email: {kai, ezra.ip}@nec-labs.com).

Z. Qi and T. Chen are with the Department of Electrical and Computer Engineering, Duke University, Durham, NC 27708, USA (email: {zhenzhou.qi, tingjun.chen}@duke.edu).

G. Zussman is with the Department of Electrical Engineering, Columbia University, New York, NY 10027, USA (email: gil@ee.columbia.edu).

D. Kilper is with the CONNECT Centre, Trinity College Dublin, Dublin 2, Ireland (email: dan.kilper@tcd.ie).

K. Asahi, H. Kageshima, and Y. Aono are with the Photonic System Development Department, NEC Corporation, Japan (email: {k-asahi, h-kageshima, jwa32}@nec.com).

## I. Introduction

Fiber optic networks have extensively been deployed across various scales, serving as the fundamental infrastructure for modern Internet backbones, telecommunication networks, and smart connected communities [2]. In addition to their capacity to deliver high-bandwidth data services with low latency, fiber-optic cables possess the capability to function as high-resolution sensors by exploiting the transducing properties of the glass medium, which make it sensitive to environmental factors such as vibration, strain, and temperature [3]–[5]. The process of fiber sensing typically involves employing an interrogator device that launches an interrogation probe signal into the fiber. As the probe signal propagates through the fiber, light scatters omnidirectionally at each position along the fiber due to Rayleigh, Brillouin, and Raman backscattering. These scattering phenomena respond differently to changes in the amplitude, phase, and frequency of the scattered light [6]–[8]. The scattered light is then collected and directed back to the interrogator for subsequent analysis and extraction of sensing information. As a result, optical networks can be naturally transformed into a distributed sensor network at scale utilizing the fiber footprint as a continuous sensing medium.

Recent advances in optical fiber sensing have enabled telecom network operators to monitor their fiber infrastructure while creating new revenue streams spanning various applications scenarios including data center interconnect (DCI), smart cities, public safety, infrastructure surveillance, intrusion detection, and seismic monitoring [4], [9]–[13]. Distributed acoustic sensing (DAS) technology has proven to be very versatile in many applications by providing distributed monitoring of vibrations and sounds along the fiber network. In addition, analog radio-over-fiber (ARoF) is another promising technology to address the limited fronthaul capacity issue in 5G/6G mobile networks via direct transmission of analog wideband radio signals over fronthaul fibers will full centralization of radio frequency (RF) resources, analog-to-digital and digital-to-analog conversions, and baseband processing.

Using dedicated fibers for sensing may be undesirable for operators whose fiber networks are close to fully utilized for dense wavelength-division multiplexing (DWDM) transmission. It is also possible that common optical functions, such as optical switching, can be shared between sensing and communication equipment for cost reduction. To achieve this

Authorized licensed use limited to: Columbia University Libraries. Downloaded on December 02,2023 at 05:49:51 UTC from IEEE Xplore. Restrictions apply.
© 2023 IEEE. Personal use is permitted, but republication/redistribution requires IEEE permission. See https://www.ieee.org/publications/rights/index.html for more information.

This article has been accepted for publication in IEEE/OSA Journal of Lightwave Technology. This is the author's version which has not been fully edited and content may change prior to final publication. Citation information: DOI 10.1109/JLT.2023.3319166




Fig. 1: Setup of the field trial of co-propagating coherent 400 GbE, distributed acoustic sensing (DAS), and analog radio-over-fiber (ARoF) signals over Manhattan dark fiber as part of the PAWR COSMOS testbed deployed in West Harlem, NYC.

goal, it is crucial to study the coexistence of sensing (e.g., pulse-based DAS signal) and data transmission (e.g., coherent 400 GbE optics and ARoF signals) on the same DWDM network. In particular, the impact of the fiber sensing signal on the quality of transmission (QoT) [14] of the coherent 400 GbE signal, such as the pre-forward error correction (pre-FEC) and post-forward error correction (post-FEC) bit error rate (BER), should be systematically investigated. Furthermore, an integrated platform with joint sensing and communication capabilities allows the sensing system to provide advance warnings to the network management system and to facilitate optical switching to the backup route in the event of fiber cuts.

In this paper, we report field trial results investigating the co-propagation of coherent 400 GbE, DAS, and ARoF signals using field-deployed dark fibers as part of the city-scale PAWR COSMOS testbed [15]–[17], which is being deployed in a dense urban environment in West Harlem, New York City (NYC), as shown in Fig. 1. We employ programmable optical space switches and reconfigurable optical add-drop multiplexer (ROADM) graybox units deployed in the COSMOS testbed to realize different optical topologies that emulate a dense metro area network. Using the COSMOS testbed, we characterize the transmission performance of the coherent 400 GbE signal with different channel baud rates and FEC modes, and its coexistence with two types of DAS signals (pulse-based DAS and constant-amplitude DAS) and ARoF signals in adjacent DWDM channels. Measurement results show that compared to the pulse-based DAS, the constant-amplitude DAS operating at optimal power levels has minimal impact on the coherent 400 GbE QoT in real-time. Using the field trial setup, we also demonstrate a use case of DAS-informed preemptive optical path switching, where a 400 GbE signal is switched to a backup fiber route as the DAS system identifies abnormal events indicating possible outage on the original fiber link.

The rest of the paper is organized as follows. We discuss related work in Section II and describe the PAWR COSMOS testbed in Section III. Then, we present the detailed field trial setup in Section IV, followed by the measurement results and analysis in Section V and conclusions in Section VI.

## II. Related Work

Using existing telecom fiber infrastructure for static strain, vibration, and temperature sensing can provide add-on values and new revenues for telecom operators in different application domains, including public safety and smart cities. However, due to the high utilization of fiber counts for data transmission, it is undesirable to provide dedicated fiber strands just for the sensing applications. Therefore, ensuring the coexistence between sensing and data transmission on the same fiber is an important ongoing research topic [14], [18]–[20]. In [14], the nonlinear impact of the DAS interrogation signal on co-propagating data channels was investigated. Burst errors were introduced to the coherent data channels after error correction by the DAS, even though the pre-FEC BER levels remained stable. Using a modified coherent receiver DSP for data transmission, the vibration-induced optical phase change during fiber propagation can be recovered in a DWDM system without inserting a designated sensing signal [18]. This method, however, has a very coarse resolution in event localization. In [19], a constant-power optical frequency domain reflectometry (OFDR) probe signal was used to monitor a transatlantic submarine cable with live coherent data traffic, providing span-level sensing capabilities (50–60 km). Lastly, over 1,000 km of DAS range with co-propagating 10 Tb/s data transmission was demonstrated using all Raman amplification and smooth roll-offs at the rising/falling edges of interrogation pulse to mitigate nonlinearity impact [20]. In addition, coherent interferometric-based approaches have been investigated to achieve good sensing resolution and accuracy with reduced complexity in the digital signal processing pipeline [13].

In addition, the ARoF technique involves converting RF signals into optical signals for efficient transmission through fiber-optic cables and then converting them back to RF signals at the receiving end. Recently, ARoF has attracted a lot of attention as an efficient and scalable solution for the 5G/6G mobile fronthaul, due to its capability to directly transport large bandwidth RF and millimeter-wave (mmWave) signals in the pure analog form between the radio unit (RU) and centralized/distributed unit (CU/DU) [21]. Recent works have focused on direct generation and transmission of 60 GHz signals based on a variation of the optical single sideband (OSSB) and optical double sideband suppressed carrier (DSB-SC) modulation techniques [22], overcoming the laser frequency offset and phase noise in an optical heterodyne ARoF system leveraging a photonic integrated mode locked laser and advanced DSP algorithms [23], as well as RF channel and network resource allocation in ARoF networks employing

Authorized licensed use limited to: Columbia University Libraries. Downloaded on December 02,2023 at 05:49:51 UTC from IEEE Xplore. Restrictions apply.
© 2023 IEEE. Personal use is permitted, but republication/redistribution requires IEEE permission. See https://www.ieee.org/publications/rights/index.html for more information.

This article has been accepted for publication in IEEE/OSA Journal of Lightwave Technology. This is the author's version which has not been fully edited and content may change prior to final publication. Citation information: DOI 10.1109/JLT.2023.3319166



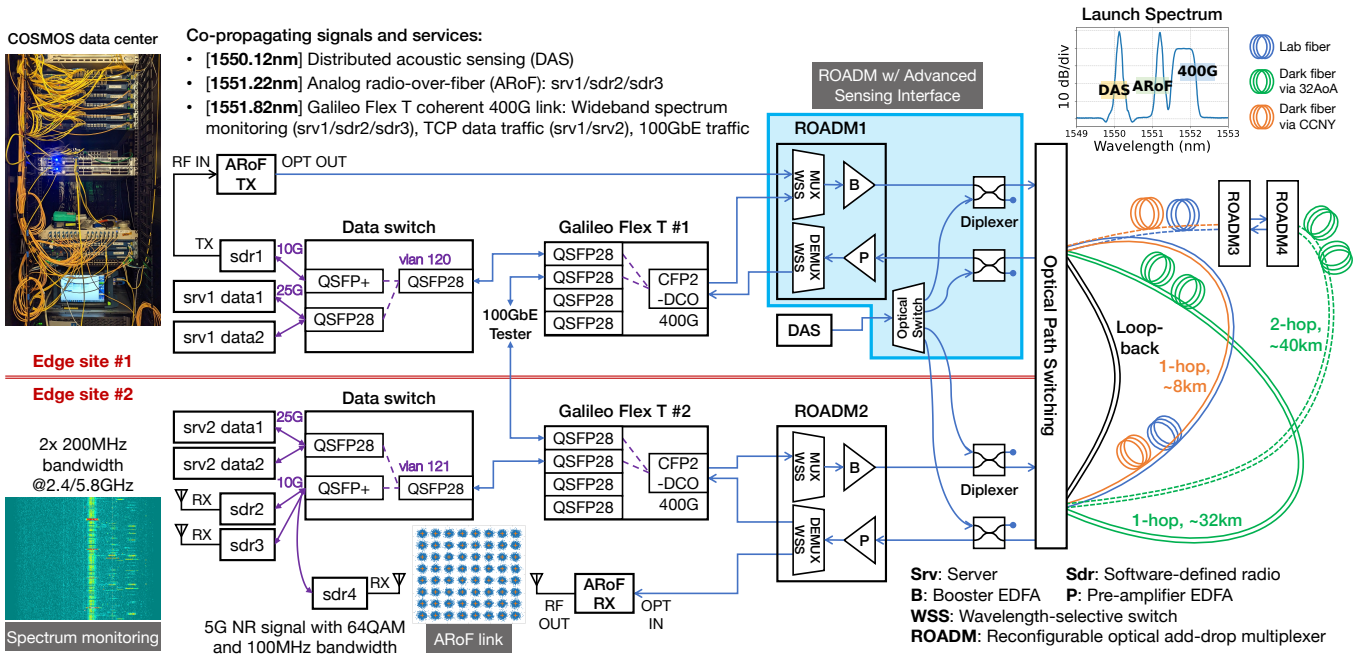


Fig. 2: Detailed experimental setup of the field trial using the COSMOS testbed with two edge sites, each of which is equipped with a Galileo Flex-T whitebox and a 400 GbE CFP2-DCO pluggable, a ROADM unit with an advanced sensing interface, and a DAS interrogator. We consider a ROADM network in a metropolitan setting with three different fiber routes, which are configured via optical path switching: (*i*) a direct loopback link, (*ii*) a 1-hop link (32 km or 8 km), and (*iii*) a 2-hop link (32 km and 8 km).

subcarrier multiplexing [24], [25]. However, the coexistence of ARoF signals with other types of signals in adjacent DWDM channels of the same fiber has not been extensively studied.

To the best of our knowledge, *this paper is the first empirical study of the coexistence of these three types of signals (DAS, coherent 400 GbE, and ARoF) with dynamic optical switching using field trial measurements in a dense urban environment*.

## III. The City-Scale PAWR COSMOS Testbed

COSMOS is a city-scale programmable testbed that is being developed and deployed in West Harlem, NYC, as part of the NSF Platforms for Advanced Wireless Research (PAWR) program to facilitate research and experimentation with advanced optical and wireless technologies in a dense urban environment [16]. In particular, the COSMOS testbed supports reconfigurable optical physical topologies using the space switching and wavelength switching capabilities enabled by a Calient S320 320×320 space switch, a DiCon 16×16 space switch, and a number of Lumentum ROADM-20 graybox units [15]. The testbed also includes lab fiber spools with varying lengths and two Manhattan dark fiber routes as depicted in Fig. 1, including a 32 km loopback route via the 32 Avenue of the Americas (32AoA), provided by ZenFi via the PAWR consortium, and an 8 km loopback route via the City College of New York (CCNY), provided by NYC and Crown Castle. In addition, COSMOS includes a larger number of software-defined radios (SDRs) with different form factors, compute servers, and data switches, which are connected to its optical network (for more details see [16]). Using COSMOS' programmable optical network, a wide range of optical front/mid/backhaul (x-haul) experiments across different layers of the networking stack can be supported, including but not limited to: erbium-doped fiber amplifier (EDFA) gain spectrum modeling and characterization [26]–[28], QoT prediction in multi-span ROADM networks [29], optical network control and cross-layering based on software-defined networking (SDN) [30], remote signal processing in cloud radio access networks (C-RANs) [31], and wireless handover supported by dynamic optical switching [32].

## IV. Field Trial Setup

The setup diagram of the field trial is shown in Fig. 2, where we consider a ROADM network with two edge sites (Edge Site #1 and Edge Site #2) that are emulated using COSMOS' programmable optical network. The setup includes a Calient S320 320×320 space switch, a DiCon 16×16 space switch, four Lumentum ROADM-20 graybox units, two dark fiber routes in Manhattan, as well as various compute and wireless components including servers, data switches, and SDRs. Each edge site includes one Galileo Flex T 400 GbE open optical transponder whitebox and a ROADM unit with an advanced sensing interface, which can be used to multiplex and demultiplex the three types of signals that co-propagate over the same fiber (see Fig. 1 for the launch signal spectrum).

**400 GbE digital coherent optics (DCO) signal**: The 400 GbE whitebox transponder, which is compliant with Telecom Infra Project's (TIP's) Phoenix requirements, consists of the NEC Network Operating System (based on the open-source Goldstone software) running on Wistron's Galileo Flex-T hardware with Lumentum 400 GbE CFP2-DCO pluggables.

Authorized licensed use limited to: Columbia University Libraries. Downloaded on December 02,2023 at 05:49:51 UTC from IEEE Xplore. Restrictions apply.
© 2023 IEEE. Personal use is permitted, but republication/redistribution requires IEEE permission. See https://www.ieee.org/publications/rights/index.html for more information.

This article has been accepted for publication in IEEE/OSA Journal of Lightwave Technology. This is the author's version which has not been fully edited and content may change prior to final publication. Citation information: DOI 10.1109/JLT.2023.3319166



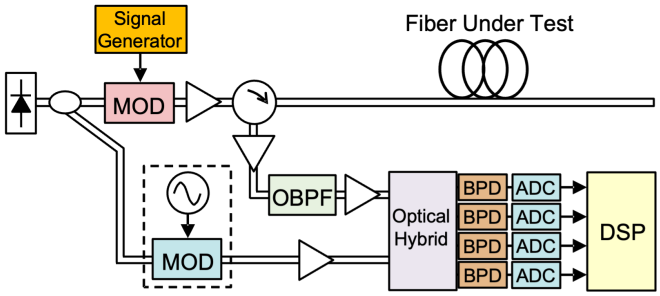


Fig. 3: Block diagram of a coherent receiver-based DAS system.

The whitebox transponder supports data rates of 100 G–400 G with flexible modulation formats and baud rates. In this field trial, we select 400 GbE transmission with dual-polarization 16QAM (DP-16QAM), which is centered at 193.1875 THz and 193.2 THz (1551.82 nm and 1551.72 nm) for the 75 GHz and 100 GHz channel width, respectively. We consider two FEC modes supported by the CFP2-DCO: open FEC (oFEC, ∼63 GBaud) and high-gain FEC (HG-FEC, ∼66 GBaud).

The 400 GbE coherent optics channel carries heterogeneous data services aggregated via the whitebox transponder and a 100 GbE data switch (Dell EMC Z9100-ON) in COSMOS through the client side 100 GbE QSFP28 ports, including:

(*i*) Parallel transmission control protocol (TCP) traffic for DCI services between two servers `srv1` and `srv2` in Edge Sites #1 and #2, respectively;

(*ii*) Digital radio baseband signals for wideband spectrum monitoring collected from two USRP X310 SDRs in Edge Site #2 (`sdr2` and `sdr3`), which monitor 200 MHz spectrum at 2.4 GHz and 5.8 GHz, respectively, and stream raw I/Q waveforms to a compute server in Edge Site #1 (`srv1`) for remote signal processing;

(*iii*) 100 GbE traffic generated by an EXFO Ethernet tester.

**Distributed acoustic sensing (DAS) signal**: The DAS signal centered at 193.4 THz (1550.12 nm) is multiplexed and demultiplexed using the advanced sensing interface on the ROADM unit, which enables simultaneous switching for communication and sensing in the same fiber. The interface utilizes low-loss optical diplexers (<0.4 dB) at the ROADM input and output line ports in conjunction with an optical switch, as shown in Fig. 2. The passband of the diplexer is centered at 193.4 THz (1550.12 nm) with 100 GHz bandwidth for DAS operation. The advanced sensing interface on the ROADM unit also allows routing of the DAS signal in the same or opposite direction as the DWDM channels for performance testing on the coherent 400 GbE signal QoT.

We use two real-time DAS systems employing different interrogation technologies in the field trial. The first one is a *pulse-based DAS*, which uses a conventional pulse interrogation scheme based on a coherent-detection Rayleigh phase OTDR [4], [9]. Using coherent detection, the DAS system recovers the full polarization and phase information of the Rayleigh backscatter from the fiber under test (FUT). The block diagram of a typical coherent receiver-based DAS system is shown in Fig. 3, where the sensing laser is also used as the local oscillator (LO) to down-convert the backscatter signal to the electric baseband. The Rayleigh backscatter field, denoted by $\mathbf{h}(t)$, can then be reconstructed from the outputs of the optical hybrid and balanced photodiodes (BPD), which corresponds to the in-phase (I) and quadrature (Q) components of the two polarizations:

$$\mathbf{y}(t) = e^{j\phi_{\text{Tx}}(t)} \cdot [x(t) \otimes \mathbf{h}(t)] + \mathbf{n}(t). \tag{1}$$

In particular, $x(t)$ is the pulse signal used for DAS interrogation, which can be generated using an electrical pulse source and an acousto-optic modulator (AOM). The optical pulse repetition (frame) rate of $R_p = 1/T_p$ is also adjusted to be longer than the round-trip propagation delay of the FUT. $\phi_{\text{Tx}}(t)$ is the phase noise of the sensing laser. The baseband electrical signals are sampled by analog-to-digital converters (ADC) and then passed through the digital signal processing (DSP) blocks implemented in the field-programmable gate array (FPGA). After digital filtering and parallelization of the data in two polarizations $x$ and $y$, the differential phase beating of Rayleigh scatters at different locations (index $n$) and timestamp (index $m$) can be computed as

$$\zeta_{ij}[n,m] = y_i[n,m] \cdot y_j^*[n-\Delta_g, m], \ \forall (x,y), \tag{2}$$

where $\Delta_g$ is the delay value that emulates a differential gauge length of $z_g = \Delta_g \cdot [c/(2n_{\text{eff}})]/T_s$ with $n_{\text{eff}}$ and $T_s$ being the fiber effective index and sampling period, respectively. $\Delta_g$ along with the pulse width can be adjusted in the DSP block to allow tuning of the spatial resolution and sensitivity of the DAS interrogator. After the combination of all the phase-beating pairs $(i,j)$ and producing one single complex-valued vector output $\zeta[n,m]$, the fiber strain at different location-time pairs $[n,m]$ can be estimated by taking the unwrapped phase $\theta[n,m] = \angle\zeta[n,m]$.

We also use another real-time constant-amplitude *chirp-pulse DAS* system in the field trial, which employs a similar hardware design and DSP algorithm as that used in [20]. In particular, chirped pulse is used as the probe signal, which is generated using a DAC and an optical IQ modulator:

$$c(t) = \sqrt{P_{\text{sens}}} \cdot \exp\left(j2\pi \cdot R_c \cdot \frac{t^2}{2}\right) \cdot \text{rect}\left(\frac{t}{T_c}\right), \tag{3}$$

where $T_c$ and $R_c$ denote the chirp duration and chirp rate, respectively, and the instantaneous frequency is $f(t) = R_c \cdot t$. The chirped pulse has a bandwidth of $B = R_c T_c$, and its autocorrelation is given by

$$R_{cc}(t) = (T_c - |t|) \cdot \text{sinc}\left(R_c \cdot t(T_c - |t|)\right). \tag{4}$$

The spatial resolution for the chirp-pulse DAS system is defined by the width of the autocorrelation function, $T = 1/(R_c T_c) = 1/B$, which can achieve the same level of resolution as the conventional pulse-based DAS with a pulse width of $T$. Using the autocorrelation property of the chirp-pulse, the Rayleigh impulse response of the optical fiber can be recovered by performing the correlation operation $c(t) * \mathbf{y}(t)$ in the DSP. The SNR gain of the chirp-pulse DAS system is then given by the "code length", $N_c = T_c/T$. The real-time DSP is implemented on the FPGA with two 1 Gsps DAC channels and four 250 Msps ADC channels. With a chirp duration of $T_c = 50\,\mu$sec and an effective chirp bandwidth

Authorized licensed use limited to: Columbia University Libraries. Downloaded on December 02,2023 at 05:49:51 UTC from IEEE Xplore. Restrictions apply.
© 2023 IEEE. Personal use is permitted, but republication/redistribution requires IEEE permission. See https://www.ieee.org/publications/rights/index.html for more information.

This article has been accepted for publication in IEEE/OSA Journal of Lightwave Technology. This is the author's version which has not been fully edited and content may change prior to final publication. Citation information: DOI 10.1109/JLT.2023.3319166



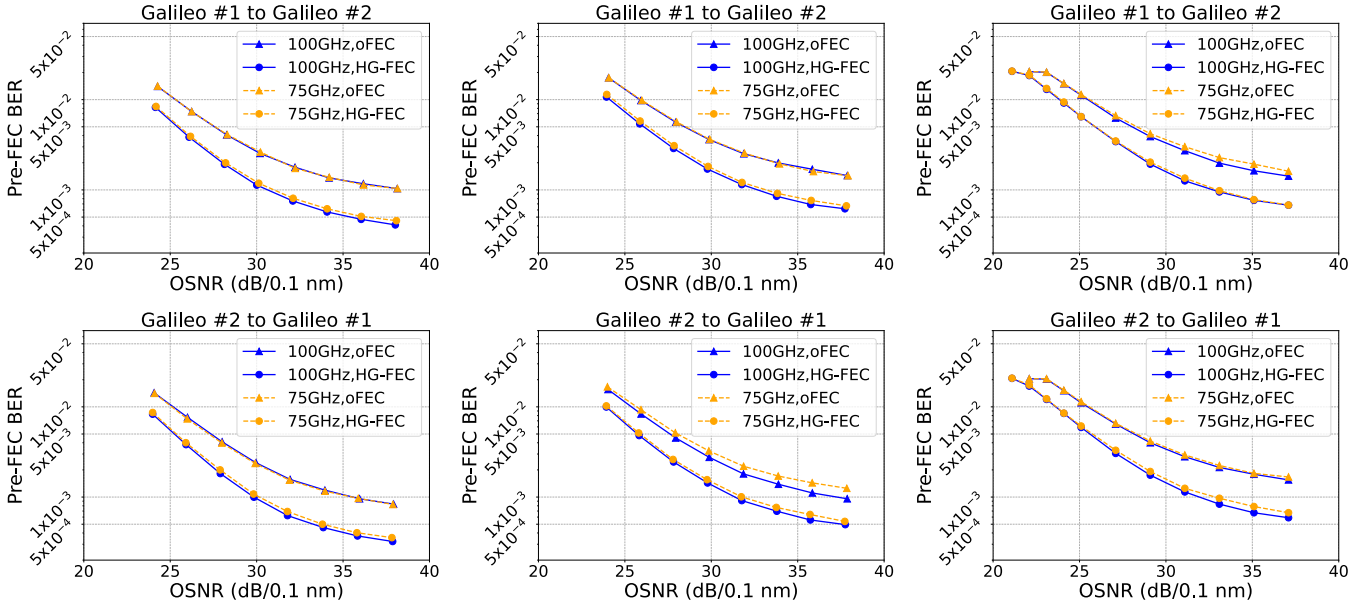


a Back-to-back link. b 1-hop link (32 km). c 2-hop link (32 km and 8 km).

Fig. 4: Coherent 400 GbE QoT over three fiber routes as shown in Fig. 2: pre-FEC BER with different ROADM channel widths (75 GHz and 100 GHz) and FEC modes (oFEC and HG-FEC).

of $B = 10$ MHz, the designed coding gain of the system is 27 dB. In addition to using chirp-pulse for DAS interrogation, the system also generates out-of-band chirp signals (not used for interrogation) outside of the chirp duration $T_c$ to maintain a constant signal amplitude (*constant-amplitude DAS*) [33].

During the field trial using the COSMOS testbed, we set the pulse width of the pulse-based DAS and the effective autocorrelation width of the chirp-pulse DAS to be the same of 100 nsec, so that both DAS systems have a comparable spatial resolution of 10 m. In addition, both systems are configured to have an interrogation frame rate of 2 kHz to support the monitoring of up to ∼50 km fiber distance for metro networks.

**Analog radio-over-fiber (ARoF) signal**: The ARoF signal centered at 193.2625 THz (1551.22 nm) is multiplexed and demultiplexed by the ROADM under through a 50 GHz channel at the MUX WSS and DEMUX WSS, respectively. In particular, a linear electro-absorption modulator (Optilab LT-12-E-M 12 GHz Lightwave Transmitter, ARoF TX in Edge Site #1) is used to modulate the RF signal generated by a USRP N310 SDR (`sdr1` in Edge Site #1). The bias voltage of the electro-absorption modulator is optimized to achieve the desired linearity performance for the modulating RF signal at maximum TX power. We consider a 5G new radio (NR) physical downlink shared channel (PDSCH) signal with 100 MHz bandwidth (sampled at 122.88 MHz) and a Physical layer based on orthogonal frequency-division multiplexing (OFDM) with 64QAM modulation on each subcarrier. This ARoF signal sent over the fiber route is detected using an amplified PIN photodiode receiver (Optilab PR-12-B-M 12 GHz PhotoReceiver, ARoF RX in Edge Site #2) connected to a remote antenna, which is then received by another USRP N310 SDR (`sdr4` in Edge Site #2) and processed at a server (`sdr2`) to obtain the error vector magnitude (EVM) of the wireless signal constellation. The wireless link SNR is controlled by adjusting the TX gain of `sdr1`.

## V. Experimental Results

In this section, we present the measurement results and analysis from the field trial using the COSMOS testbed.

### A. Baseline Coherent 400 GbE Transmission QoT

We first consider a single 400 GbE coherent channel with the channel launch power optimized at +3 dBm. Fig. 4 shows the measured pre-FEC BER of the 400 GbE signal for receiver OSNR-sweep measurements in both directions across three considered topologies (see Fig. 2): (*i*) back-to-back fiber link between the two ROADM units, (*ii*) 1-hop field fiber route (32 km), and (*iii*) 2-hop field fiber route (32 km and 8 km). We test two ROADM WSS channel widths (75 GHz and 100 GHz) and two FEC modes provided by the Galileo whitebox transponder (oFEC and HG-FEC). The results show that HG-FEC achieves better OSNR tolerance than oFEC. Compared to the back-to-back scenario, a slight performance degradation on the pre-FEC BER is observed for the coherent 400 GbE signal sent over the 1-hop and 2-hop fiber routes. An OSNR limit over the 2-hop route is measured at 22.1 dB and 23.2 dB in both directions, respectively. Across all three considered topologies, the pre-FEC BER exhibits a minimal difference when the 400 GbE signal is sent on the 75 GHz and 100 GHz channels due to ROADM WSS filtering effect. In the rest of the coexistence experiments, we apply HG-FEC and use 75 GHz channel width for the 400 GbE signal.

Authorized licensed use limited to: Columbia University Libraries. Downloaded on December 02,2023 at 05:49:51 UTC from IEEE Xplore. Restrictions apply.
© 2023 IEEE. Personal use is permitted, but republication/redistribution requires IEEE permission. See https://www.ieee.org/publications/rights/index.html for more information.

This article has been accepted for publication in IEEE/OSA Journal of Lightwave Technology. This is the author's version which has not been fully edited and content may change prior to final publication. Citation information: DOI 10.1109/JLT.2023.3319166



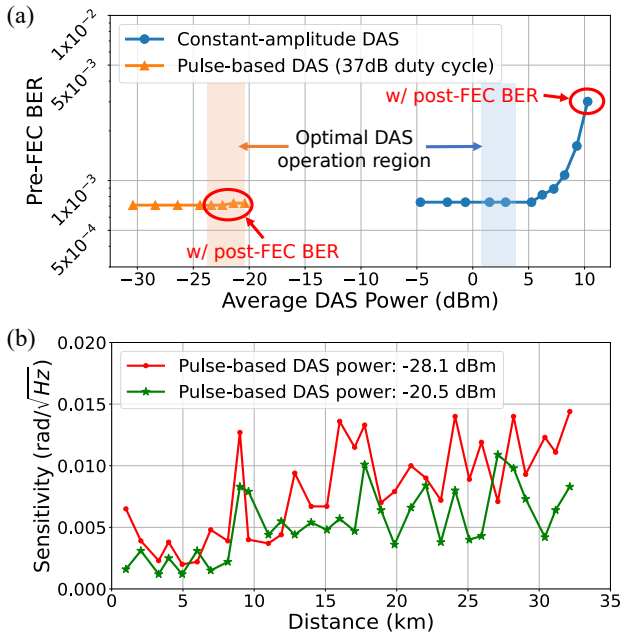


Fig. 5: (a) Impact of the pulse-based and constant-amplitude DAS interrogators on the 400 GbE QoT, (b) Sensitivity of the pulse-based DAS at two different transmit power levels.

### *B. Co-existence of Coherent 400 GbE, DAS, and ARoF Signals*

Using the field trial setup, we investigate the system performance when three signals co-propagate over the 32 km fiber route via 32AoA (see Fig. 2). Fig. 5(a) shows the measured pre-FEC BER when the DAS channel propagates in the *same direction* as the 400 GbE coherent channel, where the launch power of the DAS interrogation signal is swept while the 400 GbE coherent channel power is kept constant at +3 dBm. The ARoF signal is sent into the fiber with a launch power level of +3 dBm. Due to different DAS interrogation waveforms, pulse-based DAS operates optimally at a higher peak power (+15 dBm with 37 dB duty cycle) compared to that of the constant-amplitude DAS (+3 dBm) at longer fiber distances. Note that the average power of the pulse-based DAS is much lower with a pulse duty cycle ratio of 37 dB.

The results show that although the pre-FEC BER remains unchanged at around $7.3 \times 10^{-4}$ with increased power of the pulse-based DAS, the coherent 400 GbE signal starts to exhibit uncorrected errors and observable post-FEC BER when the average pulse-based DAS power exceeds −23.4 dBm, which is still below its optimal operation region. Under such conditions, the 400 GbE client traffic is effectively shut down. Due to the low frame rate and short burst nature of pulse-based DAS, the additional errors from cross-phase modulation (XPM) are not reflected in the pre-FEC BER, but could still cause service interruptions as the burst errors are insufficiently randomized by the FEC interleaver. On the contrary, we are able to increase the power of constant-amplitude DAS up to +9 dBm without incurring any post-FEC bit errors, which is well beyond its optimal operation region. When the DAS is switched to the *counter-propagation direction*, we observe no impact from both DAS systems on the 400 GbE QoT for both pre-FEC and post-FEC BER. On the 8 km route, we also observe no impact from both DAS in either propagation direction, likely due to the limited nonlinear interactions on the short fiber distance.

The optimal transmit power levels for the pulse-based DAS and constant-amplitude DAS were verified previously in the lab testing environment using SSMF fiber spools, achieving around 3.6 mrad/$\sqrt{\text{Hz}}$ at 40 km and around 8.6 mrad/$\sqrt{\text{Hz}}$ at 80 km for the pulse-based DAS and constant-amplitude DAS, respectively. When operating at higher transmit power levels, fiber nonlinearity effects such as self-phase modulation (SPM) and stimulated Brillouin scattering (SBS) will start to severely impact the DAS interrogation signals, therefore limiting the sensitivity. With a sampling rate of 2 kHz, the pre-FEC BER on the 400 GbE signal introduced by the DAS after its transmit power exceeds the XPM threshold is at the level of around $4e^{-5}$, which is on average much lower than the back-to-back BER of the 400 GbE channel, thus not possible to observe in pre-FEC BER measurements. However, these errors come in a burst in a short period of time and cannot be corrected by the FEC in the real-time transceiver even with data scrambling, resulting in post-FEC BER. For constant-amplitude DAS, the impact of XPM is much more suppressed and the errors will be much more distributed. In this case, deterioration of pre-FEC BER can be observed before post-FEC BER is registered at high power. Raman related impact between the DAS and communication signals was not observed in our experience for two reasons: (*i*) fiber transmission systems only start to see the impact of Raman nonlinearity when the signal power reaches the level of +15–20 dBm, which wasn't reached in our experiments; and (*ii*) Raman interaction will be more prominent for signals across wideband bandwidth (3–5 THz if using C-band), but the frequency separation between the DAS and communication signals is only around 200 GHz in our experiments.

In addition, Fig. 5(b) shows the recovered phase signal noise floor along the 32 km field fiber route using the pulse-based DAS system to provide the sensitivity level quantitatively. The effective pulse widths for both DAS systems are around 100 ns, which translates to a minimal spatial resolution of 10 meters. The gauge length of each fiber segment was also set to around 10 meters and kept the same for all the measurements in the trial. Noise floor values were averaged between 20–100 Hz. We select relatively "quiet" locations away from subway tracks and roads for the measurement, however slight environmental noise could still create fluctuations in the measurement. Two pulse-based DAS operation power levels are used for the noise floor measurements. At −20.5 dBm, which is within the optimal operation power region for the pulse-based DAS system, the phase sensitivity in the last 5 km of the fiber route is 7.2 mrad/$\sqrt{\text{Hz}}$. At −28.1 dBm, which is a level that is safe to operate the pulse-based DAS system such that it can coexist with the coherent 400 GbE signal without creating burst errors, the DAS sensitivity deteriorates to 12.2 mrad/$\sqrt{\text{Hz}}$. The reduced sensitivity of the pulse-based DAS system is also qualitatively visualized in the waterfall plot shown in Fig. 6, where lower contrast can be observed at the end of the monitored fiber link with lower optical power. In addition, Fig. 7 shows two waterfall traces of a 5 minutes duration for

Authorized licensed use limited to: Columbia University Libraries. Downloaded on December 02,2023 at 05:49:51 UTC from IEEE Xplore. Restrictions apply.
© 2023 IEEE. Personal use is permitted, but republication/redistribution requires IEEE permission. See https://www.ieee.org/publications/rights/index.html for more information.

This article has been accepted for publication in IEEE/OSA Journal of Lightwave Technology. This is the author's version which has not been fully edited and content may change prior to final publication. Citation information: DOI 10.1109/JLT.2023.3319166



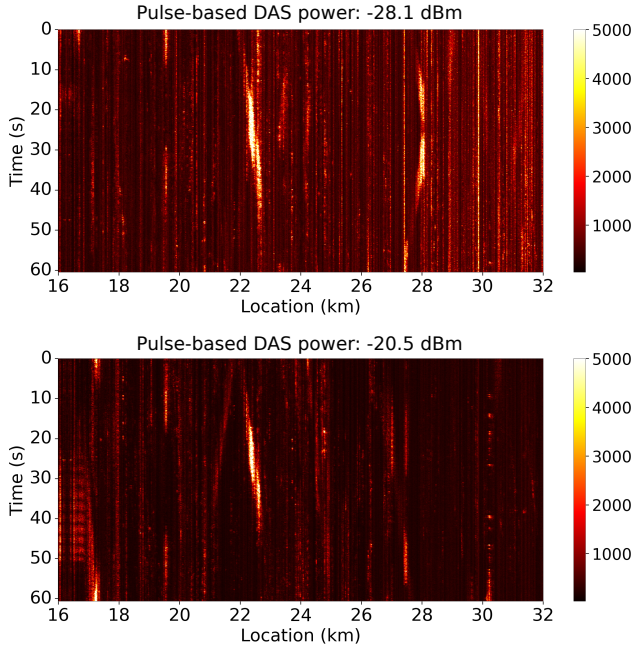


Fig. 6: DAS waterfall plots on the 32 km fiber route via 32 Avenue of the Americas (32AoA) for Manhattan traffic monitoring with different DAS transmit power levels.

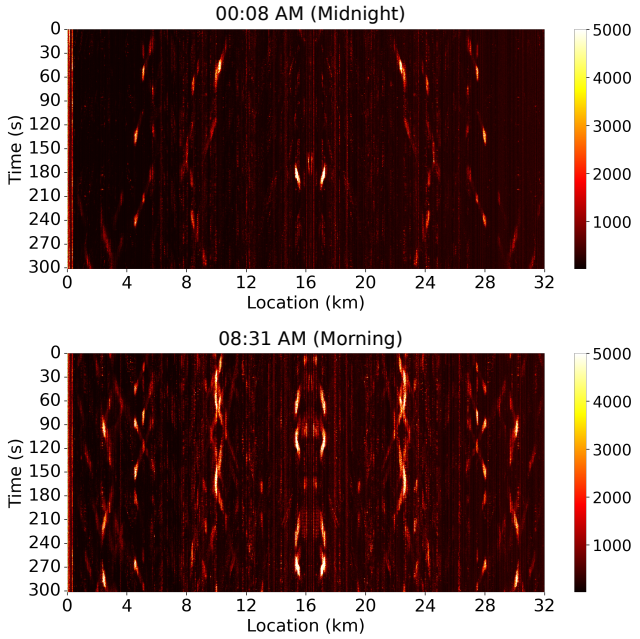


Fig. 7: DAS waterfall plots on the 32 km fiber route via 32AoA for Manhattan traffic monitoring at different times of the day.

Manhattan traffic along the 32 km fiber route at different times of the day (midnight and morning), where different traffic conditions and patterns can be observed, e.g., larger vibrations caused by subways and smaller vibrations caused by vehicles. The waterfall traces exhibit symmetry about 16 km due to the loopback configuration of the 32 km fiber route.

Finally, Fig. 8(a) shows the measured mean EVM of the co-propagating ARoF signal as a function of the wireless link SNR over different fiber routes, under a fixed received

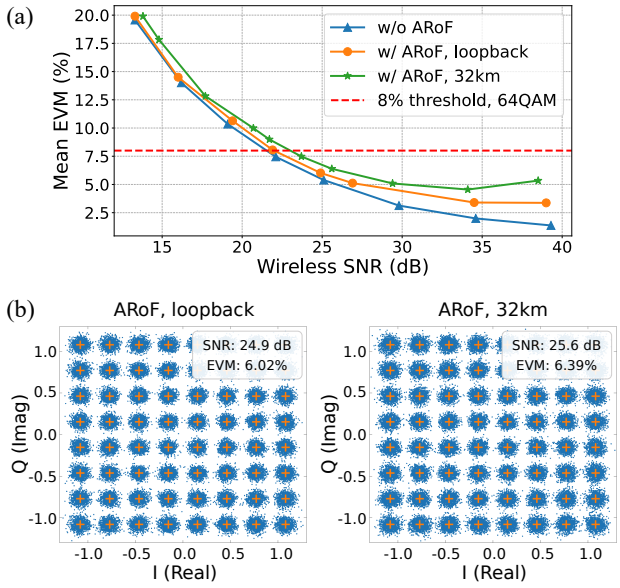


Fig. 8: (a) EVM of ARoF-based 5G NR signal with varying wireless link SNR. (b) Example received 64QAM signal constellations in a 5G NR PDSCH frame over the loopback and 32 km ARoF link.

optical power level of 0 dBm at the input to the ARoF RX. Note that the pulse-based DAS simultaneously operates at a peak transmit power level of +15 dBm with 37 dB duty cycle. The 8% threshold is the 3GPP EVM requirement for 64QAM modulation. The measurement results show slight degradation of the EVM of the 64QAM signal when the ARoF signal is sent over the 32 km route compared to scenarios where the ARoF TX and RX are connected using a short loopback fiber or without using ARoF. Fig. 8(b) shows examples of the received 64QAM signal constellation of a 5G PDSCH frame over the loopback and 32 km route, where an EVM of 6.02% and 6.39% is achieved with a wireless link SNR of 24.9 dB and 25.6 dB, respectively. In addition, no impact of the ARoF signal on the coherent 400 GbE signal QoT is observed as we sweep the launch power of the ARoF up to +10 dBm while keeping a constant launch power on the 400 GbE signal. Note that the ARoF signal used in the field trial is based on intensity modulated direct detection (IM/DD) systems, which are usually more robust against XPM compared to coherent transmission systems (e.g., 400 GbE with DP-16QAM). Therefore, the ARoF transmission performance is minimally impacted by the different DAS transmit power levels at the given channel spacing between the two signals.

### *C. Case Study: DAS-informed Optical Path Switching for Link Failure Protection*

The co-propagating DAS monitoring signal can provide protection of the coherent 400 GbE channel: by detecting abnormal event signatures preceding a link outage, alerts can be triggered for preemptive optical path switching. We demonstrate such a scenario when the constant-amplitude DAS picks up signals indicating unauthorized fiber access on the 8 km fiber route (see Fig. 6. The waterfall plot shows the vibration

Authorized licensed use limited to: Columbia University Libraries. Downloaded on December 02,2023 at 05:49:51 UTC from IEEE Xplore. Restrictions apply.
© 2023 IEEE. Personal use is permitted, but republication/redistribution requires IEEE permission. See https://www.ieee.org/publications/rights/index.html for more information.

This article has been accepted for publication in IEEE/OSA Journal of Lightwave Technology. This is the author's version which has not been fully edited and content may change prior to final publication. Citation information: DOI 10.1109/JLT.2023.3319166



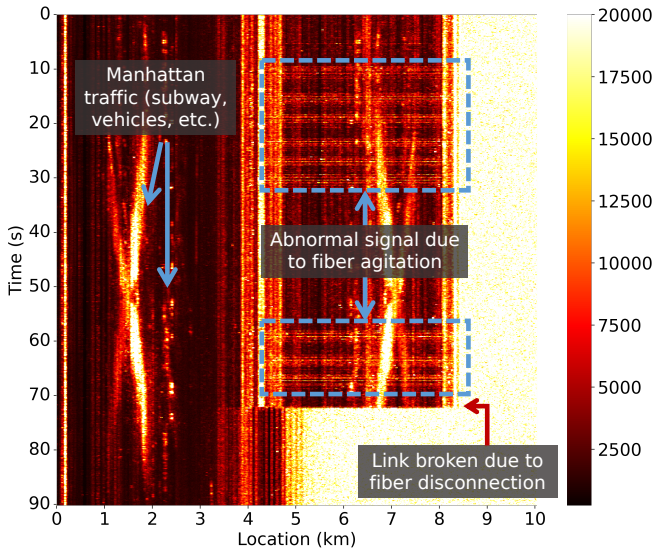


Fig. 9: DAS waterfall plots on the 8 km fiber route via CCNY before and after patch panel disconnection (fiber link failure).

strength as a function of time ($y$-axis) and fiber location ($x$-axis) with a spatial resolution of 10 meters. The vibration signal beyond the fiber end (>8.4 km) is saturated as signal extraction relies on differential optical phase interferometry and low signal amplitudes create large phase fluctuations. The 8 km fiber route is formed by a loopback cable at CCNY (see Fig. 1), thus the waterfall plot is symmetric around the loopback point at 4.2 km. When the loopback cable on the patch panel was manually agitated, bright horizontal lines can be observed as the fiber movement causes frequency shifts of the DAS chirp pulse. The signature is clearly different than other large vibration signals picked up by the DAS, such as Manhattan subways (at 1.7 km) and server room equipment vibrations (at 4.2 km). Therefore, it can be reported to the network management system as an advance warning for imminent link outages. In our demonstration, we perform an optical path switching from the 8 km fiber link (in orange) to the backup 1-hop 32 km route (in green), as shown in Figs. 1 and 2. Abnormal signals were observed by DAS monitoring during the time between 10–30 seconds and 58–70 seconds with manual agitating on the patch panel of 8 km link. This fiber link is then disconnected at the time of 72 seconds where the loss of DAS detection after 5 km as illustrated in Fig. 9. The management system optically switches the link to the backup 32 km route using the space switch interface with a switching time of ∼50 ms.

## VI. Conclusions

In this paper, we demonstrated simultaneous switching of DAS, coherent 400 GbE, and ARoF signals in adjacent DWDM channels over the same fiber via field trial in the COSMOS testbed. The coexistence of DAS, coherent 400 GbE, and ARoF signals was verified using a real-time constant-amplitude DAS, a commercial Galileo Flex T whitebox transponder, and commercial ARoF transceivers in a ROADM network with metro fibers in Manhattan, NYC. We also successfully demonstrated the use case of the switching of a 400 GbE signal to a backup route after the DAS system identifies abnormal patterns indicating imminent fiber outage.

## References

[1] Y.-K. Huang, Z. Wang, E. Ip, Z. Qi, G. Zussman, D. Kilper, K. Asahi, H. Kageshima, Y. Aono, and T. Chen, "Field trial of coexistence and simultaneous switching of real-time fiber sensing and 400GbE supporting DCI and 5G mobile services," in *Proc. IEEE/Optica OFC'23*, 2023.

[2] B. Mukherjee, "WDM optical communication networks: Progress and challenges," *IEEE J. Sel. Areas Commun.*, vol. 18, no. 10, pp. 1810–1824, 2000.

[3] E. Ip, J. Fang, Y. Li, Q. Wang, M.-F. Huang, M. Salemi, and Y.-K. Huang, "Distributed fiber sensor network using telecom cables as sensing media: Technology advancements and applications," *IEEE/Optica J. Opt. Commun. Netw.*, vol. 14, no. 1, pp. 61–68, 2022.

[4] E. Ip, F. Ravet, H. Martins, M.-F. Huang, T. Okamoto, S. Han, C. Narisetty, J. Fang, Y.-K. Huang, M. Salemi, E. Rochat, F. Briffod, A. Goy, M. del Rosario Fernández-Ruiz, and M. G. Herráez, "Using global existing fiber networks for environmental sensing," *Proc. IEEE*, 2022.

[5] B. Culshaw and A. Kersey, "Fiber-optic sensing: A historical perspective," *IEEE/OSA J. Light. Technol.*, vol. 26, no. 9, pp. 1064–1078, 2008.

[6] J. B. Ajo-Franklin, S. Dou, N. J. Lindsey, I. Monga, C. Tracy, M. Robertson, V. Rodriguez Tribaldos, C. Ulrich, B. Freifeld, T. Daley, and X. Li, "Distributed acoustic sensing using dark fiber for near-surface characterization and broadband seismic event detection," *Sci. Rep.*, vol. 9, no. 1, p. 1328, 2019.

[7] P. Lu, N. Lalam, M. Badar, B. Liu, B. T. Chorpening, M. P. Buric, and P. R. Ohodnicki, "Distributed optical fiber sensing: Review and perspective," *Appl. Phys. Rev.*, vol. 6, no. 4, p. 041302, 2019.

[8] M. Froggatt and J. Moore, "High-spatial-resolution distributed strain measurement in optical fiber with Rayleigh scatter," *Appl. Opt.*, vol. 37, no. 10, pp. 1735–1740, 1998.

[9] M.-F. Huang, M. Salemi, Y. Chen, J. Zhao, T. J. Xia, G. A. Wellbrock, Y.-K. Huang, G. Milione, E. Ip, P. Ji, T. Wang, and Y. Aono, "First field trial of distributed fiber optical sensing and high-speed communication over an operational telecom network," *IEEE/OSA J. Light. Technol.*, vol. 38, no. 1, pp. 75–81, 2019.

[10] L. Ren, T. Jiang, Z.-g. Jia, D.-s. Li, C.-l. Yuan, and H.-n. Li, "Pipeline corrosion and leakage monitoring based on the distributed optical fiber sensing technology," *Measurement*, vol. 122, pp. 57–65, 2018.

[11] G. Marra, C. Clivati, R. Luckett, A. Tampellini, J. Kronjäger, L. Wright, A. Mura, F. Levi, S. Robinson, A. Xuereb, B. Baptie, and D. Calonico, "Ultrastable laser interferometry for earthquake detection with terrestrial and submarine cables," *Science*, vol. 361, no. 6401, pp. 486–490, 2018.

[12] J. C. Juarez, E. W. Maier, K. N. Choi, and H. F. Taylor, "Distributed fiber-optic intrusion sensor system," *IEEE/OSA J. Light. Technol.*, vol. 23, no. 6, pp. 2081–2087, 2005.

[13] P. Boffi, "Sensing applications in deployed telecommunication fiber infrastructures," in *Proc. ECOC'22*, 2022.

[14] Z. Jia, L. A. Campos, M. Xu, H. Zhang, M. Gonzalez-Herraez, H. F. Martins, and Z. Zhan, "Experimental coexistence investigation of distributed acoustic sensing and coherent communication systems," in *Proc. IEEE/OSA OFC'21*, 2021.

[15] T. Chen, J. Yu, A. Minakhmetov, C. Gutterman, M. Sherman, S. Zhu, S. Santaniello, A. Biswas, I. Seskar, G. Zussman, and D. Kilper, "A software-defined programmable testbed for beyond 5G optical-wireless experimentation at city-scale," *IEEE Network*, vol. 36, no. 2, pp. 90–99, 2022.

[16] D. Raychaudhuri, I. Seskar, G. Zussman, T. Korakis, D. Kilper, T. Chen, J. Kolodziejski, M. Sherman, Z. Kostic, X. Gu, H. Krishnaswamy, S. Maheshwari, P. Skrimponis, and C. Gutterman, "Challenge: COSMOS: A city-scale programmable testbed for experimentation with advanced wireless," in *Proc. ACM MobiCom'20*, 2020.

[17] "Cloud enhanced open software defined mobile wireless testbed for city-scale deployment (COSMOS)," https://cosmos-lab.org/, 2023.

[18] G. A. Wellbrock, T. Xia, E. Ip, Y.-K. Huang, M.-F. Huang, T. Wang, and Y. Aono, "Field trial of vibration detection and localization using coherent telecom transponders over 380-km link," in *Proc. IEEE/OSA OFC'21*, 2021.

Authorized licensed use limited to: Columbia University Libraries. Downloaded on December 02,2023 at 05:49:51 UTC from IEEE Xplore. Restrictions apply.
© 2023 IEEE. Personal use is permitted, but republication/redistribution requires IEEE permission. See https://www.ieee.org/publications/rights/index.html for more information.

This article has been accepted for publication in IEEE/OSA Journal of Lightwave Technology. This is the author's version which has not been fully edited and content may change prior to final publication. Citation information: DOI 10.1109/JLT.2023.3319166




[19] M. Mazur, N. K. Fontaine, M. Kelleher, V. Kamalov, R. Ryf, L. Dallachiesa, H. Chen, D. T. Neilson, and F. Quinlan, "Advanced distributed submarine cable monitoring and environmental sensing using constant power probe signals and coherent detection," in *SubOptic*, 2023.

[20] E. Ip, Y.-K. Huang, T. Wang, Y. Aono, and K. Asahi, "Distributed acoustic sensing for datacenter optical interconnects using self-homodyne coherent detection," in *Proc. IEEE/Optica OFC'22*, 2022.

[21] S. Rommel, D. Dodane, E. Grivas, B. Cimoli, J. Bourderionnet, G. Feugnet, A. Morales, E. Pikasis, C. Roeloffzen, P. van Dijk, M. Katsikis, K. Ntontin, D. Kritharidis, I. Spaleniak, P. Mitchell, M. Dubov, J. B. Carvalho, and I. Tafur Monroy, "Towards a scaleable 5G fronthaul: Analog radio-over-fiber and space division multiplexing," *IEEE/OSA J. Light. Technol.*, vol. 38, no. 19, pp. 5412–5422, 2020.

[22] Y. Tian, K.-L. Lee, C. Lim, and A. Nirmalathas, "60GHz analog radio-over-fiber fronthaul investigations," *IEEE/OSA J. Light. Technol.*, vol. 35, no. 19, pp. 4304–4310, 2017.

[23] A. Delmade, C. Browning, T. Verolet, J. Poette, A. Farhang, H. H. Elwan, R. D. Koilpillai, G. Aubin, F. Lelarge, A. Ramdane, D. Venkitesh, and L. P. Barry, "Optical heterodyne analog radio-over-fiber link for millimeter-wave wireless systems," *IEEE/OSA J. Light. Technol.*, vol. 39, no. 2, pp. 465–474, 2020.

[24] J. Brenes, T. D. Lagkas, D. Klonidis, R. Munoz, S. Rommel, G. Landi, I. Tafur Monroy, E. Grivas, E. Pikasis, G. Bernini, J. M. Fabrega, and R. Vilalta, "Network slicing architecture for SDM and analog-radio-over-fiber-based 5G fronthaul networks," *IEEE/OSA J. Opt. Commun. Netw.*, vol. 12, no. 4, pp. B33–B43, 2020.

[25] L. Giorgi, G. Bruno, J. Nijhof, P. J. Urban, G. Vall-Llosera, F. Ponzini, and J. Ladvánszky, "Subcarrier multiplexing RF plans for analog radio over fiber in heterogeneous networks," *IEEE/OSA J. Light. Technol.*, vol. 34, no. 16, pp. 3859–3866, 2016.

[26] Z. Wang, D. C. Kilper, and T. Chen, "Open EDFA gain spectrum dataset and its applications in data-driven EDFA gain modeling," *IEEE/Optica J. Opt. Commun. Netw.*, vol. 15, no. 9, pp. 588–599, 2023.

[27] Z. Wang, D. Kilper, and T. Chen, "Transfer learning-based ROADM EDFA wavelength dependent gain prediction using minimized data collection," in *Proc. IEEE/Optica OFC'23*, 2023.

[28] E. Akinrintoyo, Z. Wang, B. Lantz, T. Chen, and D. Kilper, "Reconfigurable topology testbeds: A new approach to optical system experiments," *Opt. Fiber Technol.*, vol. 76, p. 103243, 2023.

[29] Z. Wang, E. Akinrintoyo, D. Kilper, and T. Chen, "Optical signal spectrum prediction using machine learning and in-line channel monitors in a multi-span ROADM system," in *Proc. ECOC'22*, 2022.

[30] J. Yu, C. Gutterman, A. Minakhmetov, M. Sherman, T. Chen, S. Zhu, G. Zussman, I. Seskar, and D. Kilper, "Dual use SDN controller for management and experimentation in a field deployed testbed," in *Proc. IEEE/OSA OFC'20*, 2020.

[31] M. Kohli, T. Chen, M. B. Dastjerdi, J. Welles, I. Seskar, H. Krishnaswamy, and G. Zussman, "Open-access full-duplex wireless in the ORBIT and COSMOS testbeds," in *Proc. ACM WiNTECT'20*, 2020.

[32] A. Minakhmetov, C. Gutterman, T. Chen, J. Yu, C. Ware, L. Iannone, D. Kilper, and G. Zussman, "Experiments on cloud-RAN wireless handover using optical switching in a dense urban testbed," in *Proc. IEEE/OSA OFC'20*, 2020.

[33] Y.-K. Huang, E. Ip, J. Hu, M.-F. Huang, F. Yaman, T. Wang, G. Wellbrock, T. Xia, K. Asahi, and Y. Aono, "Simultaneous sensing and communication in optical fibers," in *Proc. ECOC'22*, 2022.


Authorized licensed use limited to: Columbia University Libraries. Downloaded on December 02,2023 at 05:49:51 UTC from IEEE Xplore. Restrictions apply.
© 2023 IEEE. Personal use is permitted, but republication/redistribution requires IEEE permission. See https://www.ieee.org/publications/rights/index.html for more information.